Automatic segmentation algorithm for the extraction of lumen region and boundary from endoscopic images

H. Tian[1] T. Srikanthan[1] K. Vijayan Asari[2]

[1]Center for High Performance Embedded Systems, School of Computer Engineering, Nanyang Technological University, Singapore
[2]Department of Electrical & Computer Engineering, Old Dominion University, Norfolk, Virginia, USA

Abstract—*A new segmentation algorithm for lumen region detection and boundary extraction from gastro-intestinal (GI) images is presented. The proposed algorithm consists of two steps. First, a preliminary region of interest (ROI) representing the GI lumen is segmented by an adaptive progressive thresholding (APT) technique. Then, an adaptive filter, the Iris filter, is applied to the ROI to determine the actual region. It has been observed that the combined APT–Iris filter technique can enhance and detect the unclear boundaries in the lumen region of GI images and thus produces a more accurate lumen region, compared with the existing techniques. Experiments are carried out to determine the maximum error on the extracted boundary with respect to an expert-annotated boundary technique. Investigations show that, based on the experimental results obtained from 50 endoscopic images, the maximum error is reduced by up to 72 pixels for a 256 × 256 image representation compared with other existing techniques. In addition, a new boundary extraction algorithm, based on a heuristic search on the neighbourhood pixels, is employed to obtain a connected single pixel width outer boundary using two preferential sequence windows. Experimental results are also presented to justify the effectiveness of the proposed algorithm.*

Keywords—*Endoscopic images, Progressive thresholding, Iris filter, Heuristic search, Region detection, Boundary extraction*

Med. Biol. Eng. Comput., 2001, **39**, 8–14

1 Introduction

DETECTION of the lumen region from gastro-intestinal (GI) images is essentially a region segmentation process, and a high-speed, reasonably accurate extraction of the lumen region is needed to facilitate on-line robotic navigation for automated microrobotic endoscopy.

As the endoscope uses several light sources at its tip, and the illuminating distances of these sources are limited, the surface lying near the light source will be brighter than that lying further away. Hence, the area of lowest intensity represents the lumen region in an endoscopic image. However, lumen region absolute values are not constant, and they vary in size, shape, background illumination and reflective characteristics. Therefore a simple thresholding method involving a constant threshold value cannot be used to segment the lumen region.

There have been many algorithms developed for lumen region detection and boundary extraction, such as DEKLERCK *et al.* (1993), HEATH *et al.* (1998) and KHAN *et al.* (1992). However, these methods cannot segment the region accurately and can only obtain an approximate lumen region. To enhance the reliability of the segmented region, region growing and edge detection techniques are also proposed in ADAMS and BISCHOF (1994), GAMBOTTO (1993) and HOJJATOLESLAMI and KITTLER (1998). Moreover, WENG *et al.* (1997) mentioned a learning-based detection method, and KUMAR *et al.* (1999) applied an integrated neighbourhood search using a quad structure to try to obtain the actual boundary.

All the above methods are based on the magnitude of spatial differences, as considerable intensity differences can be expected at the boundary between an object and its background. However, the edge crisping effects are not sufficient if objects have very weak contrast to their backgrounds. Hence, they cannot guarantee high accuracy in medical images.

An adaptive progressive thresholding (APT) technique, described in ASARI *et al.* (1999), can be used for the segmentation of the lumen region. This is an iterative procedure in which the brightest homogeneous object from a given image is eliminated at each recursion, leaving only the darkest homogeneous object after the final recursion. However, for those kinds of endoscopic image whose boundaries are indistinct from the background owing to non-uniform or non-smooth surface and varying reflection, the APT technique as such is unsuitable to obtain an accurate lumen region and boundary. That necessitates

Correspondence should be addressed to H. Tian; e-mail: P141979082@ntu.edu.sg

First received 16 August 2000 and in final form 30 October 2000

MBEC online number: 20013535

the development of an effective method to detect the lumen region by enhancing complex boundaries.

A unique filter, called an Iris filter and described in KOBATAKE and MURAKAMI (1996), KOBATAKE and HASHIMOTO (1999) and KOBATAKE *et al.* (1999), can be used for the segmentation of medical images. This filter evaluates the degree of convergence of the gradient vectors within its region of support towards a pixel of interest. The degree of convergence is related to the distribution of the directions of the gradient vectors instead of their magnitudes. The output of the Iris filter is the average of the convergence indices within its region of support. The region of support of the Iris filter can change its size and shape adaptively at every pixel of interest, according to the distribution pattern of the gradient vectors surrounding it. Moreover, it has been verified that the Iris filter has much larger regions of support than most conventional filters, and it can enhance indistinct boundaries and detect regions in an image effectively, regardless of their contrast to the background.

However, the conventional Iris filter is not suitable for endoscopic images, owing to their unpredictable background illumination and irregularly shaped object boundary. This has led to the development of a new algorithm in which the APT is combined with the Iris filter to segment the complex region accurately. In this method, the APT technique is used first to extract the preliminary ROI from a grey-level image, and the region outside the ROI is considered as a constant-intensity region. Then, the modified Iris filter is employed for the enhancement and detection of the lumen region.

To extract a single pixel width connected boundary, the boundary extraction algorithm mentioned in KUMAR *et al.* (1999) employs three steps to complete the extraction process. These are the estimation of the lumen boundary according to a rule base, the application of four windows as detection operators in four separate directions and the extraction of a connected single pixel width boundary using a connecting algorithm. For complex images, where many sharp bends are present on the boundary, this algorithm cannot extract an accurate boundary. In this paper, a new boundary extraction method is proposed that consists of only two windows under a rule base. It has been shown that the algorithm has high adaptability to many images. It can obtain accurate outer boundaries of complex objects. Furthermore, it does not require any additional boundary thinning and connecting procedures, as is the case with the method proposed by KUMAR *et al.* (1999).

2 Lumen region detection and boundary enhancement

The lumen region extraction from the endoscopic images is performed in two phases. First, the APT technique is used to detect the preliminary ROI from a grey-level endoscopic image. Then, the Iris filter is applied for accurate region detection and boundary enhancement.

2.1 *Detection of preliminary ROI by APT*

APT is a modification of the statistical thresholding technique presented in OTSU (1978), similar to that suggested by CHERIAT *et al.* (1998). Consider an image of size $X \times Y$ pixels, consisting of L grey levels varying as the set $C\{0, 1, 2, \ldots, L-1\}$. Let (x, y) be the spatial location of a pixel in the image and the corresponding grey level be $I(x, y)$. Because of non-uniform illumination, the endoscopic images carry locally distributed noise that can be eliminated by passing the image through a mean smoothing filter W of size $w \times w$. This facilitates more accurate thresholding results, and thus a new intensity at the pixel location (x, y) can be given after smoothing, as follows:

$$I'(x,y) = \frac{1}{w^2} \sum_{(k,l) \in W} I(x+k, y+l) \quad \forall\ (x,y) \in X \times Y \tag{1}$$

The filtered image I' is subjected to the Otsu method, which is based on discriminant analysis that partitions the image into two classes C_0 and C_1 (e.g. objects and background) at grey level t; i.e. $C_0 = \{0, 1, \ldots, t\}$ and $C_1 = \{t+1, t+2, \ldots, L-1\}$. Let σ_B^2 and σ_T^2 be the between-class variance and total variance, respectively. An optimum threshold t^* can be obtained by maximising the between-class variance.

$$t^* = \text{Arg}\left\{ \max_{0 \le i \le L-1} (\eta) \right\} \tag{2}$$

where

$$\eta = \frac{\sigma_B^2}{\sigma_T^2} \tag{3}$$

$$\sigma_B^2 = w_0 w_1 (\mu_1 - \mu_0)^2 \tag{4}$$

$$\sigma_T^2 = \sum_{i=0}^{L-1} (i - \mu_T)^2 \frac{n_i}{M} \tag{5}$$

w_0 and w_1 denote the fraction of pixels lying in C_0 and C_1, respectively, and are given as

$$w_0 = \sum_{i=0}^{t} \frac{n_i}{M} \quad w_1 = 1 - w_0 \tag{6}$$

n_i represents the number of pixels on the ith grey level, and M is the total number of pixels in the image. μ_0 and μ_1 represent the class means for C_0 and C_1, respectively, and are calculated as

$$\mu_0 = \frac{\mu_t}{w_0} \quad \mu_1 = \frac{\mu_T - \mu_t}{1 - w_0} \tag{7}$$

where

$$\mu_t = \sum_{i=0}^{t} i \frac{n_i}{M} \quad \mu_T = \sum_{i=0}^{L-1} i \frac{n_i}{M} \tag{8}$$

The grey level t^*, which gives the maximum value of η as defined in eqn 3, is taken as the threshold. The image is further divided into two classes using t^*, and a new image $I^{(1)}$ is generated so that all the pixels in the original image having a higher grey level than t^* are excluded from $I^{(1)}$. Thus the pixels contained in $I^{(1)}$ will have a range $C^{(1)}$ given by $\{0, 1, 2, \ldots, t^*\}$. This Otsu procedure is applied recursively, and a separability factor called the Cumulative limiting factor (CLF) is used to find an appropriate threshold after each iteration. CLF for the Δth iteration is defined, similar to η, as

$$CLF(\Delta) = \frac{\sigma_B^2(\Delta)}{\sigma_T^2} \quad \text{for } \Delta \ge 1 \tag{9}$$

Here $\sigma_B^2(\Delta)$ is calculated in eqn 4 by using w_0, w_1, μ_0, and μ_1 from the progressive image $I^{(\Delta)}$ In this manner, an appropriate threshold $t^*(\Delta)$ is obtained by the maximising of the value of $CLF(\Delta)$ for the image $I^{(\Delta)}$. The iterative procedure is stopped whenever $CLF(\Delta)$ becomes smaller than an empirically determined value, such that

$$CLF(\Delta) \le \alpha \frac{\mu_T}{\sigma_T^2} \tag{10}$$

where α is a constant known as the limiting parameter, which is obtained by a great deal of experiments conducted on images taken from a particular endoscopic camera. This takes into account the light intensity and distribution of the light sources mounted on the endoscope. α should be different for each group

of images, depending on the camera lighting environment and the reflection characteristics of the objects.

2.2 *Detection of actual lumen region using Iris filter*

We have mentioned that the APT method cannot work well on an image that has very weak contrast between object and background. Moreover, the termination condition of eqn 10 is an empirical formula, and α is an estimated value determined by experiments. As a result, there can exist an estimation error that also decreases the accuracy of the lumen region detection. Therefore, in the proposed algorithm, a preliminary lumen region is extracted using the APT method, and the remaining parts of the image out of the threshold value are set as a uniform background. Then, an Iris filter is applied for accurate lumen region detection and boundary enhancement.

2.2.1 *Iris filter:* Let us denote the intensity of an image and its gradient vector at (x, y) as $I(x, y)$ and $\boldsymbol{g}(x, y)$, respectively. The Iris filter is not applied to the image itself, but rather to its gradient vector field. Here a 3×3 Prewitt operator for input images is adopted. Let us denote row and column gradients by $\boldsymbol{G_R}(x, y)$ and $\boldsymbol{G_C}(x, y)$, respectively. The gradient amplitude of $\boldsymbol{g}$ is given by

$$|\boldsymbol{g}(x, y)| = [\boldsymbol{G_R}(x, y)^2 + \boldsymbol{G_C}(x, y)^2]^{\frac{1}{2}} \tag{11}$$

and the orientation of $\boldsymbol{g}$ with respect to the row axis is

$$\phi(x, y) = \tan^{-1} \frac{\boldsymbol{G_C}(x, y)}{\boldsymbol{G_R}(x, y)} \tag{12}$$

The region of support of the Iris filter R_p is a union of N half-lines radiating from the pixel of interest P, as shown in Fig. 1. We define the convergence index of the gradient vector $\boldsymbol{g}$ at a point Q_i towards the pixel of interest as follows:

$$f(\boldsymbol{g}|x', y') = f(Q_i) = \begin{cases} \cos\theta, & |\boldsymbol{g}| \neq 0 \\ 0, & |\boldsymbol{g}| = 0 \end{cases} \tag{13}$$

where Q_i is an arbitrary pixel on the ith half-line, whose relative co-ordinates from the pixel of interest are denoted by (x', y'), and θ is the orientation of the gradient vector $\boldsymbol{g}$ at Q_i with respect to the ith half-line.

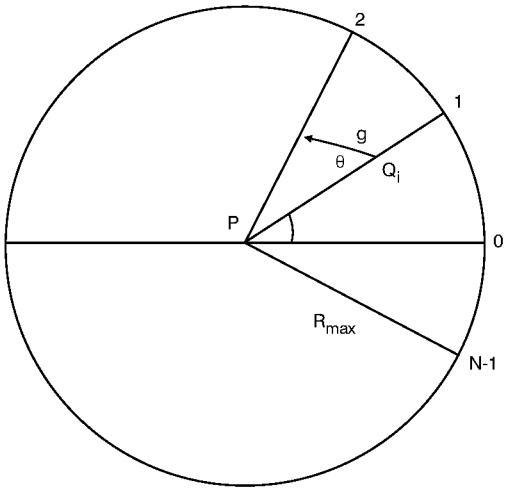

Fig. 1 *Region of support R_p*

The maximum convergence index $C_i(x, y)$ of gradient vectors on the ith half-line can be defined as follows:

$$C_i(x, y) = \max_{Q_i} \frac{\int_P^{Q_i} \cos\theta(x', y')dl}{\overline{PQ_i}} \quad 0 < \overline{PQ_i} < R_{max} \tag{14}$$

The output of the Iris filter at the pixel of interest (x, y) is defined as average $C_i(x, y)$

$$C(x, y) = \frac{1}{N} \sum_{i=0}^{N-1} C_i(x, y) \tag{15}$$

The output value of the Iris filter falls between -1 and $+1$.

2.2.2 *Combining APT and Iris filter:* Although the Iris filter can enhance and detect rounded convex regions of various sizes and contrasts effectively and has many advantages compared with other conventional filters. It is not suitable for endoscopic images, mainly because of the following problems:

- The Iris filter should be used in a uniform background image, whereas, for endoscopic images, the lumen region is the object. Hence, all the parts around it should be regarded as background. However, these regions are non-smooth, with many curves and varying reflection characteristics. Furthermore, the distribution of the gradient vector is disordered in the whole image.
- Although the Iris filter is very powerful in enhancing the indistinct boundary, it is time-consuming, because $\cos\theta$ is computed for the whole gradient image on a pixel by pixel basis. Hence, it is not well suited for real-time image processing.

To overcome these problems, the APT technique is incorporated into a conventional Iris filter to identify the object with a complex background accurately. The final output intensity image $I^{(\Delta)}$ from APT, denoted as $I(x, y)$ at the spatial location (x, y), is regarded as the input image to the Iris filter. It can be observed from the GI images that some curved surfaces have darker levels too. They also form some unwanted black regions in the output of APT that are to be suppressed. An additional constraint on the selection of a region of support R_P excluding a central area with radius R_{min} can be incorporated into the conventional Iris filter. This constraint implies that the optimum location of Q_i that maximises the convergence index given by eqn 14 must be sought in the concentric ring area between $R_{min} \leq \overline{PQ_i} \leq R_{max}$. By selecting a suitable minimum length R_{min} of the half-line in the Iris filter, the unwanted parts can be eliminated, and the true lumen region can be enhanced at the same time.

3 Boundary extraction algorithm based on heuristic search

Owing to non-uniform mucosal reflections, the lumen consists of small sub-regions of relatively higher intensities that form irregular white pockets embedded in the main lumen region of the Iris filter's output. To eliminate these and to obtain the actual boundary, a boundary extraction algorithm is proposed.

The boundary extraction procedure, which is based on the spatial locations of the pixels, is divided into two parts. The search starts from the top right pixel of the lumen region, i.e. the pixel with the minimum y co-ordinate and maximum x co-ordinate. From the initial pixel, a top-left and top-down preferential search is conducted, using the sequence window shown in

Fig. 2*a*. The numbers in the Figure represent the preferential sequence in which neighbourhood pixels are searched. If a boundary pixel is found in the neighbourhood, it is included into a new boundary array and eliminated from the original boundary to avoid the repeated inclusion of the same pixel. Then the new boundary pixel is checked in the same preferential sequence. This procedure is continued until the pixel location having maximum y is reached. Then, in the same way, another search is made to obtain a single pixel width boundary from bottom-right and bottom-up pixels, using the preferential sequence window shown in Fig. 2*b*. However, most of the regions of the image are normally more complex than a smooth and regular one. For example, during the top-left and top-down search, there may be left-to-right and bottom-up directions also. A similar situation occurs during the bottom-right and bottom-up search. In addition to the preferential sequential search of the Fig. 2*a* window for the top-left and top-down search, the following set of rules are also employed to obtain the accurate boundary of the object region. Here, the co-ordinate of the boundary pixel under consideration is assumed to be (x, y).

- If $(x-1, y-1)$ is found, check for $(x+1, y-1)$ and $(x, y-1)$. If $(x+1, y-1)$ is present, then it is a boundary pixel. Else, if $(x, y-1)$ is present, then it is a boundary pixel. Else $(x-1, y-1)$ is a boundary pixel.
- If $(x+1, y)$ is found, then it is a boundary pixel, and pixel $(x, y-1)$ is eliminated.
- If $(x+1, y-1)$ is found, then it is a boundary pixel, and pixels $(x, y-2)$ and $(x, y-1)$ are eliminated.
- If $(x, y-1)$ is found, then it is a boundary pixel, and pixels $(x-1, y-2)$, $(x-1, y-1)$ and $(x-1, y)$ are eliminated.
- If all neighbourhoods cannot be found, consider $(x-1, y-1)$ as a boundary pixel.

A similar rule base can be used for the Fig. 2*b* window, for the bottom-right and bottom-up search.

- If $(x+1, y+1)$ is found, check for $(x-1, y+1)$ and $(x, y+1)$. If $(x-1, y+1)$ is present, then it is a boundary pixel. Else, if $(x, y+1)$ is present, then it is a boundary pixel. Else $(x+1, y+1)$ is a boundary pixel.
- If $(x-1, y)$ is found, then it is a boundary pixel, and pixel $(x, y+1)$ is eliminated.
- If $(x-1, y+1)$ is found, then it is a boundary pixel, and pixels $(x, y+2)$ and $(x, y+1)$ are eliminated.
- If $(x, y+1)$ is found, then it is a boundary pixel, and pixels $(x+1, y+2)$, $(x+1, y+1)$ and $(x+1, y)$ are eliminated.
- If all neighbourhoods cannot be found, consider $(x+1, y+1)$ as a boundary pixel.

These constraints ensure that the two windows change the sequence priority adaptively, according to the different directions during the search, so that an accurate and effective outer boundary can be obtained.

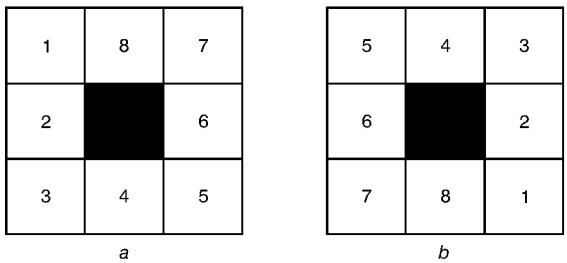

Fig. 2 *Boundary extraction preferential sequence: (a) window for top-left and top-down; (b) window for bottom-right and bottom-up*

4 Experimental results and discussion

To verify the results of the proposed segmentation technique, experiments were conducted on a large set of endoscopic images (i.e. 50 images). The images of the GI tract were captured by an endoscope consisting of a miniature CCD camera having a resolution of 200 000 pixels. The typical size of the processed image was restricted to 256×256 pixels. MATLAB (version 5.3) with the Image Processing Toolbox (version 2.2) was used on a PC platform* to carry out the simulations.

First, a grey-level image consisting of 256 grey levels was generated from the original colour image, and an averaging filter of size 3×3 was used to smooth the image. Then, the APT technique was applied to find the preliminary ROI. Here, the limiting parameter α was chosen to be 40 (obtained by experiments). The preliminary regions thresholded by APT are shown in Figs 3*b*, *f*, *j* and *n*, corresponding to the endoscopic images shown in Figs 3*a*, *e*, *i* and *m*. The optimum values of threshold and *CLF*, along with the number of iteration steps performed in APT for these images, are shown in Table 1.

The ROI obtained by APT was then regarded as the input to the Iris filter. The pixels in the ROI were given the same grey level as in the original image. The row and column gradients were obtained using the Prewitt operator with 3×3 pixels, and the orientation of each gradient vector was computed using eqn 12. The number of half-lines N of the Iris filter was taken as 36. These half-lines, which are equi-spaced in angle by $2\pi/36$, were mapped onto 36 sets of lattice points. The row and column co-ordinate of the qth pixel from the pixel of interest on the ith half line is denoted by $([r_{iq}], [c_{iq}])$. The symbols $[r_{iq}]$ and $[c_{iq}]$ represent maximum integers less than or equal to the real numbers r_{iq} and c_{iq}, respectively, and they are defined as follows:

$$r_{iq} = r - q \sin \frac{\pi}{18} i \tag{16}$$

$$c_{iq} = c + q \cos \frac{\pi}{18} i \tag{17}$$

where (r, c) are the row and column co-ordinates of the pixel of interest. Then the output of the practical Iris filter in the discrete space is

$$C(r, c) = \frac{1}{36} \sum_{i=1}^{36} C_{imax} \tag{18}$$

where the convergence index, defined by eqn 14, is modified to

$$C_{imax} = \max_{R_{min} \le n \le R_{max}} \frac{1}{n} \sum_{q=1}^{n} \cos \theta_{iq} \tag{19}$$

where n is the number of pixels in the ith half-line. The angle θ_{iq} is the orientation of the gradient vector with respect to the ith half-line, at the qth pixel from the pixel of interest.

The computation of $\cos \theta_{iq}$ is time consuming, especially when the region of interest is large. To reduce the computation time, the maximum radius of the region of support of the Iris filter R_{max} is set equal to the maximum radius of the ROI. It can also obtain better enhancement of the ROI.

In certain cases, unwanted small black regions can appear in the final output of APT, owing to the presence of curved surfaces having darker levels in the image. These will be regarded as noise that should be suppressed. We can detect their radius automatically and set the value as R_{min}. Then, the optimum location of Q_i will be searched in the range $R_{min} \le \overline{PQ}_i \le R_{max}$,

* Pentium III, 500 MHz.

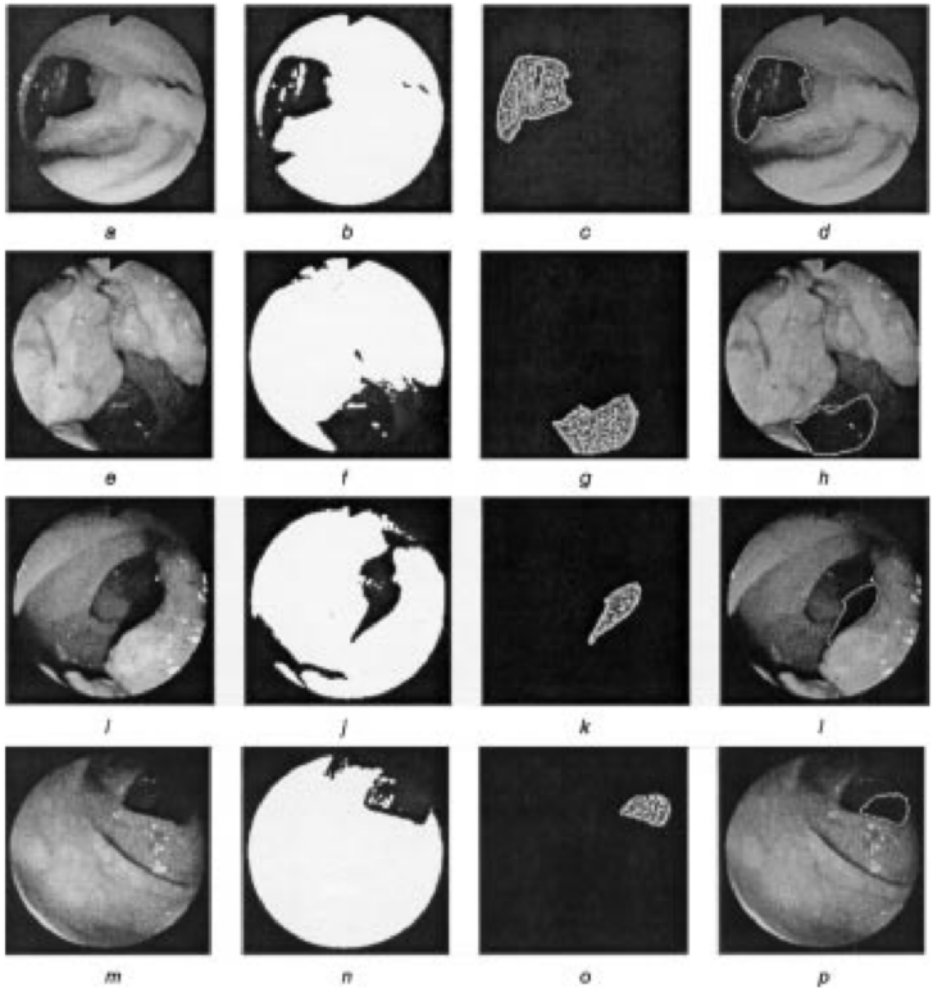

Fig. 3 *Boundary extraction: (a)(e)(i)(m) original images; (b)(f)(j)(n) output of APT; (c)(g)(k)(o) output of combined APT-Iris filter technique; (d)(h)(l)(p) boundaries obtained using the proposed boundary extraction algorithm*

as stated in eqn 19. The R_{max} and R_{min} values chosen for this set of experiments are shown in Table 2.

The lumen regions segmented by using the combined APT–Iris technique are shown in Figs 3*c*, *g*, *k* and *o*. Then a connected single pixel width boundary is obtained by applying the new boundary extraction technique described in Section 3. The extracted lumen boundaries are shown in Figs 3*d*, , *l* and *p*. The corresponding boundary lengths for the four images were obtained as 308 pixels, 260 pixels, 184 pixels and 150 pixels. To verify the effectiveness of the boundary extraction algorithm, another set of binarised images with more complex outer boundaries were used. The extracted boundaries of these images are shown in Fig. 4.

A comparison between the proposed segmentation technique and the method presented in KUMAR *et al.* (1999) is shown in Table 3. The accuracy comparison is performed by measuring the maximum absolute distance between corresponding points on an expert annotated boundary and the boundary obtained by the computer techniques.

Table 1 Parameter selection for preliminary region segmentation by APT

	Optimum value of *CLF*	Optimum threshold *t**	Iteration steps
Fig. 3*b*	0.7789	33	47
Fig. 3*f*	0.8075	40	49
Fig. 3*j*	0.6504	25	55
Fig. 3*n*	0.7041	20	60

Fig. 5 shows the error comparison results for the 50 typical endoscopic images. It is evident from the results that the combined APT–Iris filter technique provides a more accurate lumen region and boundary. This technique displays its unique efficiency when the lumen region has a weak contrast with respect to the other parts of the image. The maximum error on the extracted boundary with respect to an expert-annotated boundary has been reduced by up to 72 pixels in the experimental results obtained from 50 endoscopic images.

5 Conclusions

A new lumen region detection algorithm for endoscopic images based on a combination of adaptive progressive thresholding and the Iris filter has been presented. It has been shown that an accurate lumen region can be obtained by applying the combined APT–Iris filter technique. It helps to enhance the indistinct boundary of the region of interest.

A new boundary extraction algorithm based on a heuristic search is also presented. It has been demonstrated that a

Table 2 Support region parameters of Iris filter

	R_{max}	R_{min}
Fig. 3*c*	82	5
Fig. 3*g*	88	6
Fig. 3*k*	79	16
Fig. 3*o*	82	1

Table 3 Comparison of lumen region and boundary extraction from endoscopic images

		KUMAR *et al.* (1999)	Proposed technique
Lumen region detection and boundary enhancement	applied to ROI obtained enhancement	intensity image APT quad structure based *INS* + back projection	gradient fields APT Iris filter
Continuous single pixel width boundary extraction	redundant pixels numbers of windows connecting	many 4 required	none 2 not required
Accuracy		normal	very high
Speed (MATLAB 5.3 with Image Processing Toolbox on Pentium III, 500 MHz)		420 s	741 s

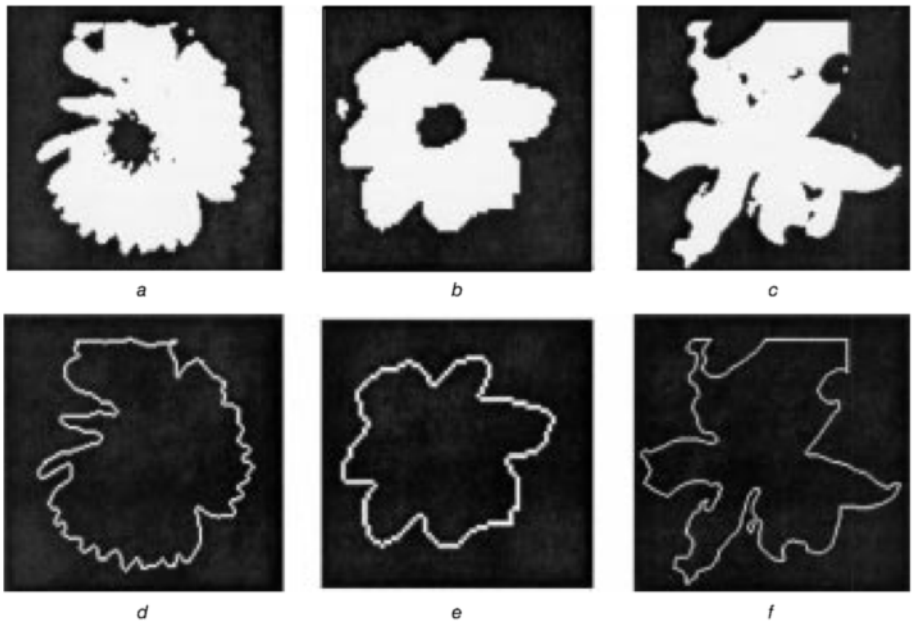

Fig. 4 *Boundary extraction: (a), (b) and (c) binarised images; (d), (e) and (f) boundaries obtained using the proposed boundary extraction algorithm*

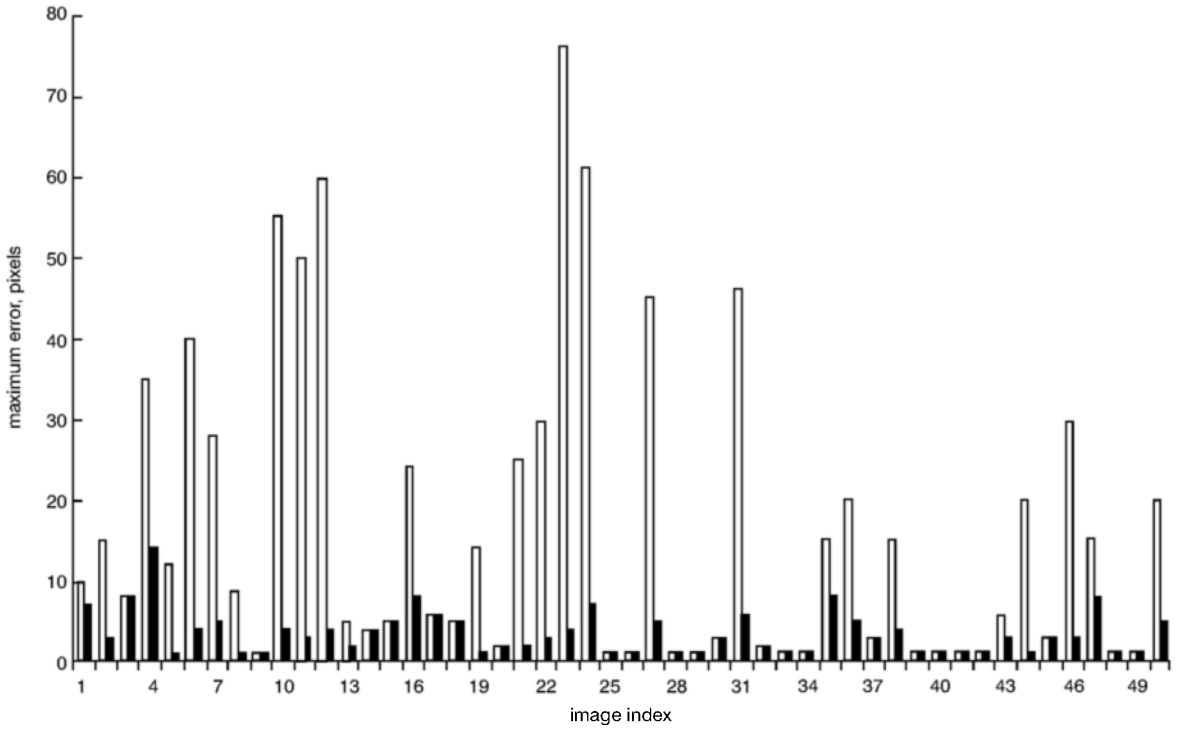

Fig. 5 *Maximum error on the boundary obtained by combined APT-Iris filter (■) and KUMAR's method (□) with respect to an expert annotated boundary*

single pixel width connected boundary of the region can be determined using the proposed boundary extraction method. Simulation results confirm that the new method is suitable to any shape of the outer boundary of the region, and it precludes the need for a separate boundary connecting algorithm. Finally, experimental results for various endoscopic images validate the effectiveness of the proposed method for images with complex outer boundaries.

Acknowledgments—The authors wish to thank Ms Yangxin, of the School of Electrical & Electronics Engineering, Nanyang Technological University, Singapore, for providing the test image database for the experiments.

References

ADAMS, R., and BISCHOF, L. (1994): 'Seeded region growing', *IEEE Trans. Pattern Anal. Mach. Intell.*, **16**, pp. 641–647

ASARI, K. V., SRIKANTHAN, T., KUMAR, S., and RADHAKRISHNAN, D. (1999): 'A pipelined architecture for image segmentation by adaptive progressive thresholding', *Microprocess. Microsyst.*, **23**, pp. 493–499

CHERIAT, M., SAID, J. N., and SUEN, C. Y. (1998): 'A recursive thresholding technique for image segmentation', *IEEE Trans. Image Process.*, **7**, pp. 918–921

DEKLERCK, R., CORNELIS, J., and BISTER, M. (1993): 'Segmentation of medical images', *Image Vis. Comput.*, **11**, pp. 486–503

GAMBOTTO, J. P. (1993): 'A new approach to combining region growing and edge detection', *Pattern Recog. Lett.*, **14**, pp. 869–875

HEATH, M., SARKAR, S., SANOCKI, T., and BOWYER, K. (1998): 'Comparison of edge detectors', *Comput. Vis. Image Underst.*, **69**, pp. 38–54

HOJJATOLESLAMI, S. A., and KITTLER, J. (1998): 'Region growing: a new approach', *IEEE Trans. Image Process.*, **7**, pp. 1079–1084

KHAN, G. N., and GILLIES, D. F. (1992): 'Parallel-hierarchical image partitioning and region extraction' in SHAPIRO, L., and ROSENFIELD, A. (Eds): 'Computer vision and image processing' (Academic Press, San Diego), pp. 123–140

KOBATAKE, H., and MURAKAMI, M. (1996): 'Adaptive filter to detect rounded convex regions: Iris filter'. Proc. Int. Conf. Pattern Recognition, **2**, pp. 340–344

KOBATAKE, H., and HASHIMOTO, S. (1999): 'Convergence index filter for vector fields', *IEEE Trans. Image Process.*, **8**, pp. 1029–1038

KOBATAKE, H., MURAKAMI, M., TAKEO, H., and NAWANO, S. (1999): 'Computerized detection of malignant tumors on digital mammograms', *IEEE Trans. Med. Imag.*, **18**, pp. 369–378

KUMAR, S., ASARI, K. V., and RADHAKRISHNAN, D. (1999): 'Real-time automatic extraction of lumen region and boundary from endoscopic images', *Med. Biol. Eng. Comput.*, **37**, pp. 600–604

OTSU, N. (1978): 'A threshold selection method from gray level histogram', *IEEE Trans. Syst. Man Cybern.*, **SMC-8**, pp. 62–66

WENG, J., SINGH, A., and CHIU, M. Y. (1997): 'Learning-based ventricle detection from cardiac MR and CT images', *IEEE Trans. Med. Imag.*, **10**, pp. 578–591

Authors' biographies

H. TIAN received her BSc and MEng in Computer and System Science from Xiamen University, China, in 1992 and 1995, respectively. Currently, she is working towards her PhD at the Centre for High Performance Embedded Systems, Nanyang Technological University, Singapore. Her research topic includes computer vision and image processing.

T. SRIKANTHAN has been employed at the School of Computer Engineering of Nanyang Technological University as an Associate Professor since June 1991. He is also the Director of the Centre for High Performance Embedded Systems. He received his BS in Computer and Control Systems and PhD in Electrical Engineering from Coventry University in 1981 and 1987, respectively. His research interests include computer architecture, embedded systems, image processing and high-speed arithmetic units.

K. VIJAYAN ASARI received his BSc in Electronics and Communication Engineering from the University of Kerala, and MTech. and PhD in Electrical Engineering from IIT, Madras, India. Currently, he is an Associate Professor in the Department of Electrical and Computer Engineering at Old Dominion University, USA. His research interests include computer vision, image processing and digital system architecture.